Methane to Methanethiol Conversion by FeS^+. A Combined Experimental and Theoretical Study†

Susanne Bärsch, Detlef Schröder, and Helmut Schwarz*

Institut für Organische Chemie der Technischen Universität Berlin, Strasse des 17, Juni 135, D-10623 Berlin, Germany

P. B. Armentrout*

Department of Chemistry, University of Utah, Salt Lake City, Utah 84112

Received: September 28, 2000; In Final Form: January 4, 2001

The reaction of FeS^+ with methane is examined by guided ion beam mass spectrometry and density functional theory employing the B3LYP/6-311+G* level of theory. For the FeS^+/CD_4 system examined in the experiments, two major product ions, Fe^+ and $FeSD^+$, are observed along with minor channels leading to $FeCD_3^+$, $FeSCD_3^+$, and $FeSCD^+$. All products are formed in endothermic processes. The measured thresholds for the formations of Fe^+ and $FeSD^+$ are compared with computational data as well as literature thermochemistry. In the theoretical approach, two competing reaction mechanisms for the formation of Fe^+, concomitant with neutral methanethiol, are investigated and used to interpret the experimental data. The lowest-energy path involves a formal 1,2-addition of H_3C-H across the Fe^+-S bond to generate a CH_3FeSH^+ insertion intermediate. This bond activation step involves spin inversion from the sextet to the quartet surface en route to the products. The occurrence of the second conceivable pathway resulting in formation of $HFeSCH_3^+$ as an intermediate can be ruled out because of the high-energy demand associated with overcoming the insertion barrier along this pathway.

Introduction

Sulfidic ores represent a large amount of minerals in the earth's crust and are involved in many geochemical processes.[1] Iron sulfides are of particular economic importance as inexpensive, abundant sources for pig iron as well as sulfuric acid. Further, transition-metal sulfides can be used as catalysts for chemical and petrochemical processes.[2] Compared to transition-metal oxides as the chalcogenide congener, sulfides are usually less reactive but sometimes exhibit enhanced selectivities.[3] Also, transition-metal sulfides are more resistant against poisoning than the corresponding oxide catalysts. Finally, transition-metal sulfides play important roles in biological systems.[4] The reactive centers of ferredoxins, for instance, consist of Fe_4S_4 clusters. Other Fe_mS_n and mixed metal−sulfur clusters constitute the reactive sites of various enzymes such as hydrogenases, nitrogenases, and sulfite reductases.[5]

In this paper we deal with the investigation of the chemistry of model systems for iron−sulfur compounds at a molecular level.[6−8] These studies provide first steps toward a more detailed understanding of the role of electronic structure in the more complex systems involved in solution chemistry. The advantage of gas-phase chemistry is the absence of counterions, solvent effects, and bulk phenomena, thus allowing the evaluation of the intrinsic reactivity of the organometallic systems as well as the role of electronic structures.[9−11] In passing, we note that this approach has, for instance, been used extensively in the investigation of transition-metal oxides and has contributed to a better understanding of oxidation reactions.[10,12]

The FeS^+ cation investigated in this paper can be regarded as the smallest possible model system to mimic larger iron−sulfur clusters, and its reactivity is therefore of extended interest. This work extends our previous study of the reactivity of FeS^+ in which the reactivity toward H_2 was examined by experiment and theory.[13]

Experimental and Theoretical Methods

The guided ion beam (GIB) mass spectrometer used for the experiments has been described in detail previously.[14,15] Briefly, atomic Fe^+ ions are produced in a direct-current discharge source connected to a flow tube. Inside the source, an iron cathode is held at 1.5−2.5 kV in a plasma consisting of about 90% helium and 10% argon. Ar^+ ions are produced in the discharge and accelerated toward the iron rod, thereby sputtering off neutral and ionic metal fragments. About 60 cm downstream from the discharge, FeS^+ is produced by adding carbonyl sulfide to the flow. In the remaining 40 cm of the flow tube, the ions undergo $>10^4$ thermalizing collisions at a typical flow tube pressure of ∼0.7 mbar. At the end of the tube, the ions are extracted, accelerated, and passed through a magnetic sector for reactant ion selection. The mass-selected ions are decelerated to the desired kinetic energies and focused into an rf octopole ion guide. The octopole is used to trap the reactant and product ions in the radial direction and therefore maintains good collection efficiencies at low kinetic energies. The octopole passes through a gas cell of known effective length (8.26 cm) filled with CD_4 used as the reactant at relatively low steady pressures of $(1-3) \times 10^{-4}$ mbar to ensure single-collision conditions. Unreacted parent ions and product ions drift from the reaction cell to the end of the octopole, are extracted, and are focused into a quadrupole mass filter for mass analysis and subsequent detection by a secondary electron/scintillation detector.

† Dedicated to Professor Jürgen Troe on the occasion of his 60th birthday.

10.1021/jp0035380 CCC: $20.00
Published on Web 02/21/2001

Laboratory ion energies (E_{lab}) are converted into center-of-mass energies (E_{CM}) using $E_{CM} = E_{lab}M/(M + m)$, where M and m are the corresponding reactant neutral and ion masses, respectively. The absolute energy scale and the corresponding full width at half-maximum (fwhm) of the ion beam kinetic energy distribution are determined as described in previous publications.[14] The beams have Gaussian kinetic energy distributions with an average fwhm of ca. 0.24 eV in the laboratory frame. The uncertainty in the absolute energy scale is ±0.05 eV (lab). Details for the conversion of raw ion intensities into cross sections are outlined elsewhere.[14a] Absolute cross sections are estimated to be correct within ±20%.

Data analysis has been performed according to the following procedure. Cross sections are modeled using the following equation:[14c,d]

$$\sigma(E) = \sigma_0 \sum g_i (E + E_i - E_0)^n / E \qquad (1)$$

where E denotes the relative translational energy, E_0 is the reaction threshold, σ_0 is an energy-independent scaling factor, and n is a fitting parameter. The summation over rovibrational energy levels i with energies E_i and relative populations g_i explicitly includes the internal energies of polyatomic reactants. Relative populations g_i are obtained from Maxwell−Boltzmann distributions of vibrational energy levels at 300 K, calculated using the Beyer−Swinehart algorithm.[15] The vibrational frequencies of CD_4 are taken from ref 16, and that of FeS^+ is calculated as 463 cm^{-1} at the B3LYP/6-311+G* level of theory (see below). After convolution of the model over the kinetic energy distributions of the reactants, the parameters σ_0, n, and E_0 are optimized to best reproduce the data using a least-squares criterion. Reported errors in E_0 comprise the range of values obtained for several data sets and the absolute uncertainty of the energy scale. Equation 1 inherently assumes that all of the internal energy is capable of coupling into the reaction coordinate, an assumption that has been shown to lead to accurate thermochemistry in numerous cases.[14c,d,17−19]

Computations are performed on either IBM/RS 6000 workstations or a CRAY-YMP supercomputer. For the calculations of geometries and energies, the B3LYP[20] density functional theory/HF (hybrid functional) is applied, combined with 6-311+G* basis sets[21,22] as implemented in the Gaussian94 program package.[23] For reasons outlined below, geometry optimization of one particular transition structure is only achieved at the B3LYP/6-311G level of theory. However, it has been shown for other TSs that modifications in the basis set from 6-311G to 6-311+G* induce only relatively small changes in geometries and relative energies. Single-point energy calculations at the B3LYP/6-311+G* level of theory allow comparison to the relative energetics of the remaining parts of the potential-energy surface (PES). All stationary points are characterized as minima or first- or higher-order saddle points by evaluation of the frequencies and normal modes. Further, several pathways between the transition structures and their corresponding minima were characterized by internal reaction coordinate (IRC) calculations.[24] Corrections for zero-point vibrational energy (ZPVE) are included, if not stated otherwise. The computed rotational constants and the unscaled vibrational frequencies are used for conversion of 0 K to 298 K data.

The B3LYP approach is used because it has been shown to provide reasonably accurate geometries and relative energetics for organometallic systems while having modest computational demands.[25,26] Specifically, investigations of the related FeS^+/H_2 system[13] using the same approach unraveled information concerning the pathways of product formation. The averaged error of the relative energies calculated with B3LYP has been estimated to be about ±0.3 eV for coordinatively unsaturated iron compounds.[25] Calculations of atoms or atomic ions may be associated with larger errors because of the known deficiency of the B3LYP approach to describe the low-spin/high-spin separations in 3d atoms properly. This behavior is attributed to an artificial preference of $3d^n$ configurations over $3d^{n-1}4s^1$ configurations.[25,27] For example, the B3LYP/6-311+G* level of theory predicts $Fe^+(^4F,3d^7)$ to be 0.18 eV more stable than $Fe^+(^6D,4s^13d^6)$, whereas spectroscopy[28] determines that the Fe^+ cation has a ^6D ground state 0.25 eV lower in energy than the ^4F first excited state. Despite the erroneous ground-state assignment of the atom, the relative energies given below refer to the $Fe^+(^6D)$ asymptote.

Results

In this section, we first briefly discuss earlier results related to the FeS^+/CH_4 system and then present an experimental investigation of the deuterated variant of this system studied in a guided ion beam mass spectrometer. The use of fully deuterated methane in the GIB experiments reduces mass overlap between the products because of the limited mass resolution of the quadrupole analyzer in the GIB instrument. Differences in zero-point energies therefore yield slightly different thresholds compared to the computationally investigated, unlabeled system. For comparison with the perprotio system, calculated zero-point energies of the labeled and unlabeled species are used to adjust the experimental thresholds. The presentation of the experimental results is followed by a discussion of the calculated PES of the FeS^+/CH_4 system. In particular, different routes for the activation of CH_4 by FeS^+ are investigated. In analogy to our previous study on the FeS^+/H_2 system,[13] kinetic isotope effects as well as tunneling phenomena are neglected.

In earlier mass spectrometric experiments, no reaction of FeS^+ with methane was observed under thermal conditions.[29] It can thus be concluded that all products of the reaction of $FeS^+ + CH_4$ are formed endothermically or that their formation is hindered by considerable barriers. Instead, the reverse reaction of Fe^+ and methanethiol leads to formation of $FeSCH_2^+$ and FeS^+ ions (branching ratio of 59:41).[29,30] Formation of FeS^+ from Fe^+ and methanethiol corresponds to the reverse of the title reaction, while formation of $FeSCH_2^+$ is not observed in this work.

Experimental Results. The reaction of FeS^+ with CD_4 in the GIB apparatus yields five ionic products formed in the following reactions:

$$FeS^+ + CD_4 \rightarrow Fe^+ + CD_3SD - 0.86\ eV \qquad (2a)$$

$$\rightarrow Fe^+ + S + CD_4 - 3.09\ eV \qquad (2b)$$

$$\rightarrow FeCD_3^+ + SD - 1.76\ eV \qquad (3)$$

$$\rightarrow FeSD^+ + CD_3 - 1.27\ eV \qquad (4)$$

$$\rightarrow FeSCD^+ + D_2 + D \qquad (5)$$

$$\rightarrow FeSCD_3^+ + D \qquad (6)$$

The results are analogous to the major products observed in the reaction of FeO^+ with [D_4]methane as investigated by several experimental techniques.[31] The thermochemical data given in

TABLE 1: Heats of Formation and Dissociation Energies for Ionic and Neutral Species at 0 K[a]

species	$\Delta_f H_0$ (eV)	D_0 (eV)	species	$\Delta_f H_0$ (eV)	D_0 (eV)
H	2.24		D	2.28	
S	2.85 ± 0.87				
H_2	0.0	4.48	D_2	0.0	4.55
SH	1.48 ± 0.03		SD	1.50 ± 0.03	
CH_3[b]	1.55 ± 0.004		CD_3[c]	1.47 ± 0.04	
CH_3S[b]	1.36 ± 0.02		CD_3S[c]	1.28 ± 0.02	
CH_4	-0.77 ± 0.004		CD_4[c]	-0.92 ± 0.004	
CH_3SH[d]	-0.24 ± 0.004		CD_3SD[e]	-0.30 ± 0.004	
Fe^+	12.15 ± 0.78				
FeS^+[f]	11.90 ± 0.87	3.09 ± 0.04			
Fe^+-SH[g]	10.77 ± 0.14	2.86 ± 0.11	Fe^+-SD[g]	10.78 ± 0.14	2.86 ± 0.11
Fe^+-CH_3[h]	11.33 ± 0.05	2.37 ± 0.05	Fe^+-CD_3[e]	11.25 ± 0.05	2.37 ± 0.05
Fe^+-Cl[h]	9.94 ± 0.13	3.45 ± 0.11			
HCl	-0.95 ± 0.004	4.43 ± 0.004			

[a] Taken from Chase, M. W., Jr.; Davies, C. A.; Downey, J. R., Jr.; Frurip, D. J.; McDonald, R. A.; Syverud, A. N. *J. Phys. Chem. Ref. Data* **1985**, *14* (Suppl. 1) (JANAF tables), except as noted. [b] Berkowitz, J.; Ellison, G. B.; Gutman, D. *J. Phys. Chem.* **1994**, *98*, 2744. [c] These values for the deuterio compound were obtained from the difference between protio and deuterio species obtained from footnote d. The difference was subtracted from the JANAF value for the protio species. [d] Lias, S. G.; Bartmess, J. E.; Liebman, J. F.; Holmes, J. L.; Levin, R. D.; Mallard, W. G. *J. Phys. Chem. Ref. Data* **1988**, *17* (Suppl. 1). [e] A procedure similar to that in footnote c is applied; however, as the thermochemistry of the deuterio species is not tabulated, we assume the difference between protio and deuterio species is additive from the contributions of each component, e.g., the difference between CH_3SH and CD_3SD forms from adding up the contributions of CH_3 vs CD_3 and SH vs SD. [f] Schröder, D.; Kretzschmar, I.; Schwarz, H.; Rue, C.; Armentrout, P. B. *Inorg. Chem.* **1999**, *38*, 3474. [g] Reference 13. [h] Reference 9c.

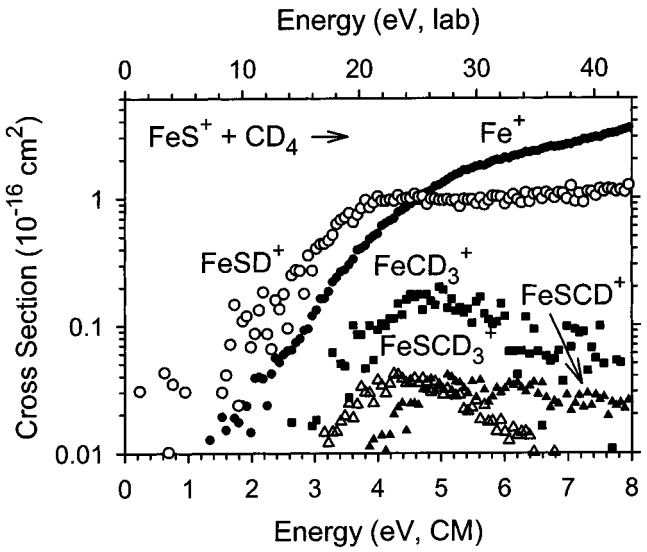

Figure 1. Product distributions obtained in the reaction of FeS^+ with CD_4 as a function of kinetic energy in the center-of-mass (lower axis) and laboratory (upper axis) frames. Products include Fe^+ (●), $FeSD^+$ (○), $FeCD_3^+$ (■), $FeSCD_3^+$ (△), and $FeSCD^+$ (▲).

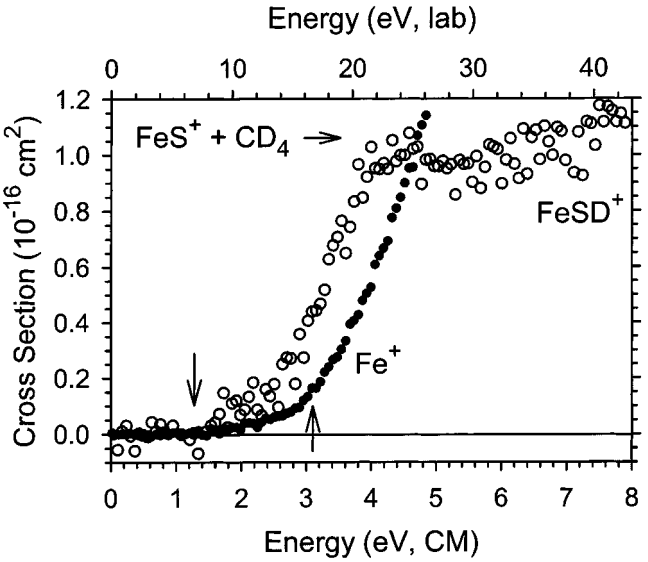

Figure 2. Product cross sections for the reaction of FeS^+ with CD_4 to form Fe^+ (●) and $FeSD^+$ (○) as a function of kinetic energy in the center-of-mass (lower axis) and laboratory (upper axis) frames. Arrows indicate the thermodynamic threshold for $FeSD^+$ production at 1.27 eV and for $Fe^+ + S + CD_4$ at 3.09 eV.

reactions 2−4 are calculated using the 0 K heats of formation and bond dissociation energies collected in Table 1 and refer to the species in their electronic ground states.

Figure 1 gives an overview of the product distribution as a function of the relative kinetic energy of the reactant ions. Clearly, the Fe^+ and $FeSD^+$ products dominate the reaction. Compared to our earlier study on FeS^+/H_2, the present system is slightly richer in possible product channels; however, the number of conceivable intermediates is about an order of magnitude larger. We therefore will focus on a concise discussion of only the two most abundant products, Fe^+ and $FeSD^+$. The onsets of the experimental cross sections of these two reactions are depicted in more detail in Figure 2 and are further evaluated below. The cross sections of the remaining products $FeCD_3^+$, $FeSCD_3^+$, and $FeSCD^+$ are small ($\sigma_{max} = 0.2$ Å^2), and hence, the data are scattered. While refraining from a rigorous quantitative analysis, qualitatively the $FeSCD^+$ channel rises where the $FeSCD_3^+$ product starts decreasing rapidly. It may therefore be assumed that $FeSCD^+$ evolves by dehydrogenation of $FeSCD_3^+$. Further information about the minor product channels can be obtained by combining our experimental and theoretical work (see below).

Let us now discuss the two major product channels, starting with the formation of Fe^+ in reactions 2a and 2b. Analysis of the Fe^+ cross section with eq 1 can only be achieved by assuming bimodal behavior. The first process dominates up to about 3 eV, above which a faster rising, second process takes over, Figure 2. Analysis of the threshold region yields $E_0 = 1.19 \pm 0.19$ eV (Table 2). Note that this result is in line with literature thermochemistry for the formation of Fe^+ and CD_3SD as the neutral counterpart, reaction 2a. The threshold of the second feature in the cross section is analyzed to be $E_0 = 3.02 \pm 0.16$ eV. This threshold is consistent with the tabulated bond dissociation energy for FeS^+ ($D_0 = 3.09 \pm 0.04$ eV),[7k] thus implying that this feature results from simple collision-induced dissociation (CID) of FeS^+ according to reaction 2b.[32]

TABLE 2: Summary of the Parameters in Eq 1 Used for the Fits of the Cross Sections

reaction	E_0, eV	σ_0	n
$FeS^+ + CD_4 \rightarrow Fe^+ + CD_3SD$ (2a)[a]	1.19 ± 0.19	0.06 ± 0.03	2.1 ± 0.3
$FeS^+ + CD_4 \rightarrow Fe^+ + S + CD_4$ (2b)[a]	3.02 ± 0.16	1.4 ± 0.2	1.8 ± 0.1
$FeS^+ + CD_4 \rightarrow FeSD^+ + CD_3$ (4)[b]	1.27	0.2	1.0

[a] The E_0 values are the average of several threshold fits with uncertainties of 1 standard deviation. [b] Model of the assumed first feature of the $FeSD^+$ data channel with a fixed $E_0 = 1.27$ eV, calculated from literature thermochemistry.

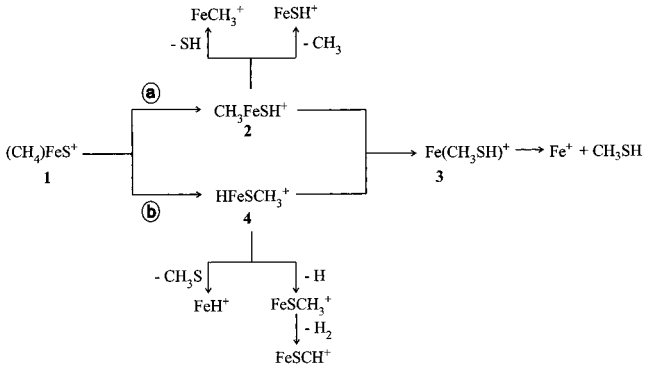

Figure 3. Schematic description of the two calculated reaction pathways ⓐ and ⓑ of the $[Fe,S,C,H_4]^+$ system. Note that only the minima are displayed; transition structures that connect the minima are omitted for the sake of simplicity and are discussed in the text.

Although the $FeSD^+$ product is less abundant than Fe^+ at elevated energies ($\sigma_{max} \approx 1.2$ Å^2 for $FeSD^+$ compared to $\sigma_{max} \approx 3$ Å^2 for Fe^+), it dominates over the Fe^+ product at energies below 4 eV. Unfortunately, the data for $FeSD^+$ formation are strongly scattered in the threshold region. The reason for the high noise level in the $FeSD^+$ product is the proximity in mass to the parent ion beam of FeS^+, which has a much higher intensity. As the $FeSD^+$ thermochemistry is known,[13] we refrain from a rigorous quantitative analysis of the $FeSD^+$ channel. In a more qualitative sense, formation of $FeSD^+$ occurs at an apparent threshold consistent with the 1.27 ± 0.16 eV value expected from literature thermochemistry (Figure 2). However, the cross section rises slowly from this threshold and then increases more rapidly above about 3 eV. A rationale for this behavior is presented further below.

Theoretical Results. Our theoretical investigation of the FeS^+/CH_4 system includes two conceivable reaction mechanisms that differ by the orientation of Fe and S relative to the C−H bond being activated (Figure 3). Both mechanisms commence with formation of the encounter complex **1**, followed by insertion of FeS^+ into one C−H bond to afford the intermediate CH_3FeSH^+ (**2**) or $HFeSCH_3^+$ (**4**). From both intermediates, the reaction may continue forward toward formation of $Fe(CH_3SH)^+$ (**3**). However, direct dissociations of **2** and **4** are also feasible (Figure 3). The complexity of the PES analysis is further increased because two spin surfaces need to be considered for the following reasons: (i) The calculated energy difference of the low-lying sextet and quartet states of FeS^+ is only 0.22 eV.[7g] (ii) The analogous oxygen system, FeO^+/CH_4, involves both the sextet and quartet PESs.[33] In the next section, the structures of the stationary points in the FeS^+/CH_4 system are presented briefly (Chart 1). For the sake of simplicity, the notation used throughout this paper gives the spin multiplicities as superscripts preceding the formula while neglecting orbital symmetries; e.g., the sextet ground state of $FeS^+(^6\Sigma^+)$ is referred to as $^6FeS^+$.

Reactants. In agreement with earlier results,[7g,13,34] our calculations predict a $^6\Sigma^+$ ground state for FeS^+ represented by a $1\sigma^2 2\sigma^2 1\pi^4 1\delta^2 2\pi^2 3\sigma^1$ occupation of the valence orbitals in a one-configuration picture. The calculated ground-state bond dissociation energy of 3.12 eV agrees favorably with the established literature value of 3.09 ± 0.04 eV.[7k] However, this agreement is most likely a result of fortuitous error cancellation considering the erroneous assignment of ground-state Fe^+ in the B3LYP approach.[35] The lowest-lying quartet state FeS^+-($^4\Pi$) is only 0.22 eV higher in energy than the ground state. Calculations on the methane molecule yield the expected tetrahedral symmetry with a $^1A_1$ ground state. In the following, all calculated energies will be given with respect to the $^6FeS^+ + CH_4$ asymptote ($E_{rel} = 0.0$ eV), if not stated otherwise.

Encounter Complex. Starting from the reactants, the first minimum along both reaction pathways is the encounter complex **1**. Of the different orientations that can be thought of, only the η^3-iron-bound structures ^{4}**1** and ^{6}**1** are identified as minima along the PESs for both spin states (Chart 1). Even though sulfur-bound methane complexes may still exist, it is reasonable to assume that iron-bound structures such as **1** are energetically most favorable. The latter is rationalized in an ion/induced dipole picture because the iron end of the FeS unit carries the larger positive charge ($q_{Fe} = 0.64$) and thus interacts more strongly with the methane molecule. Although the calculations predict a sextet ground state (^{6}**1**) at $E_{rel} = -0.71$ eV, the quartet analogue (^{4}**1**) is very close in energy ($E_{rel} = -0.64$ eV). This narrow splitting renders the assignment of the ground state ambiguous. Calculations of ^{6}**1** indicate that the CH_4 moiety is bound to iron at a distance $r_{FeC} = 2.17$ Å with a SFeC angle of 139.5°. The quartet complex, ^{4}**1**, shows a quasi-linear arrangement of FeS^+ and the methane molecule ($\alpha_{SFeC} = 177.8°$), with the CH_4 unit at nearly the same distance ($r_{FeC} = 2.19$ Å). These iron−carbon bond lengths correspond to purely electrostatic bonding, as is expected for a closed-shell ligand such as methane. We note in passing that the PES for movement of the methane unit around Fe^+ is very shallow; i.e., changes in α_{SFeC} of 20° require less than 0.05 eV. Given the energetic and geometric similarities of ^{4}**1** and ^{6}**1** in conjunction with the flatness of the potential in this region, it seems likely that the sextet and quartet surfaces interact strongly, and facile interconversion is expected.

Reactions of the CH_3FeSH^+ Intermediate (Figure 3, Path ⓐ). The encounter complex **1** and the insertion structure **2**, CH_3FeSH^+, are connected by TS**1/2** (Chart 1). The sextet and quartet TSs (^{6}TS**1/2** and ^{4}TS**1/2**) are theoretically localized at $E_{rel} = 0.85$ and 0.59 eV, respectively. Structurally, both TSs are quite similar, having planar, four-membered rings. The imaginary modes (^{6}TS**1/2**, $\nu = i1575$ cm^{-1}; ^{4}TS**1/2**, $\nu = i1382$ cm^{-1}) correspond to the hydrogen migrations from the carbon to the sulfur atom. In the sextet TS, the Fe−S bond and the C−H distance of the migrating hydrogen atom are notably longer than in the quartet TS ($r_{FeS} = 2.14$ Å and $r_{CH} = 1.62$ Å for ^{6}TS**1/2** vs $r_{FeS} = 2.06$ Å and $r_{CH} = 1.48$ Å for ^{4}TS**1/2**). This suggests that the quartet TS has stronger bonds with more perfect pairing, thus explaining its lower energy demand. After passing through TS**1/2**, the reaction reaches the insertion species, CH_3FeSH^+ (**2**) with a quartet ground state (^{4}**2** at $E_{rel} = -0.59$ eV) and a low-lying sextet state (^{6}**2** at $E_{rel} = -0.35$ eV). The quartet

CHART 1

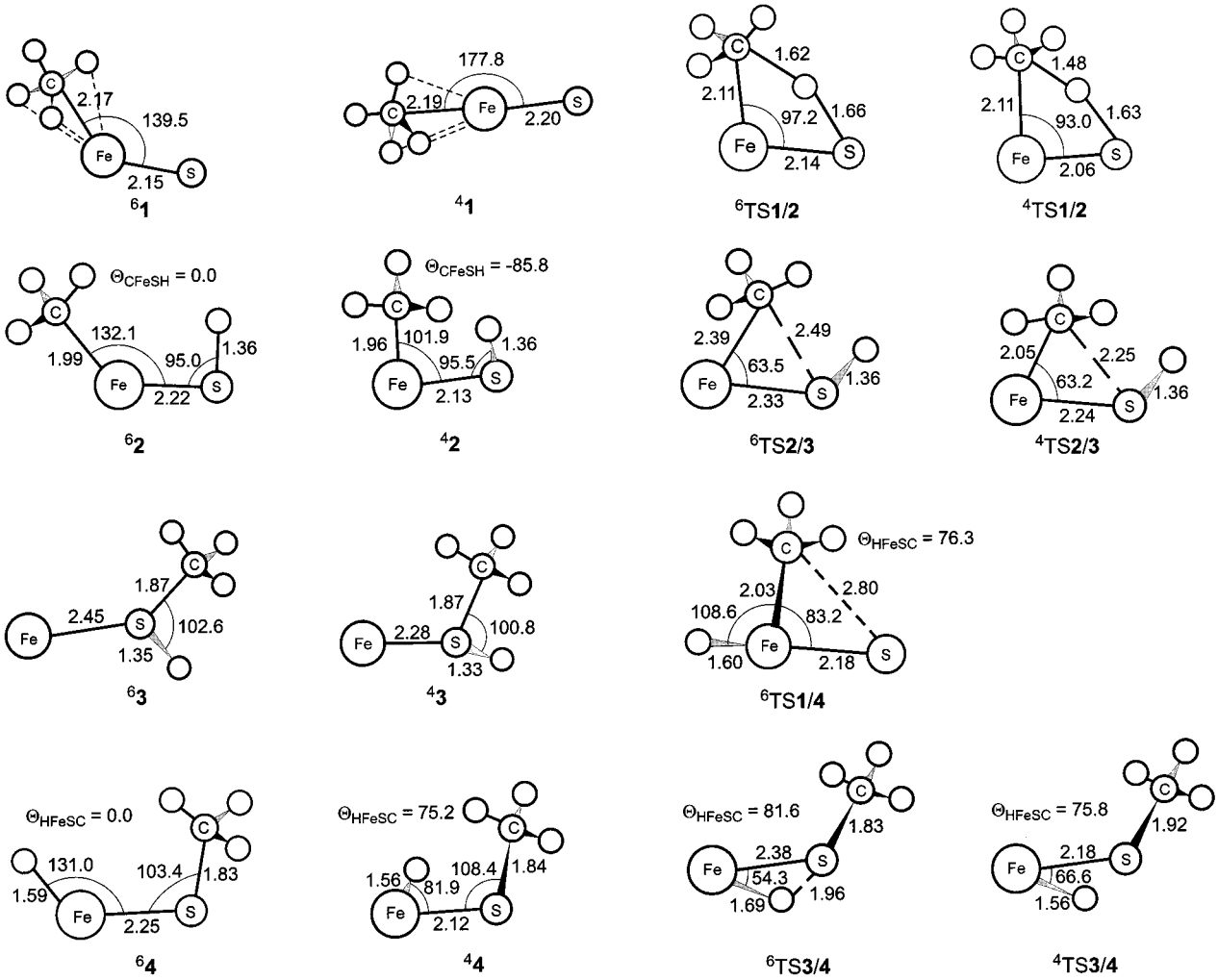

structure is distinctly nonplanar, showing a dihedral angle of $\theta_{CFeSH} = -85.8°$, whereas the corresponding sextet is planar in this respect, $\theta_{CFeSH} = 0.0°$. From **2**, the reaction continues via TS**2/3** to the methanethiol complex **3** as the most stable species on the part of the FeS^+/CH_4 surface studied here. The TSs depicted in Chart 1 are located at $E_{rel} = -0.03$ and $+1.19$ eV on the quartet and sextet PESs, respectively. The imaginary frequencies of i525 and i386 cm^{-1} for ^{4}TS**2/3** and ^{6}TS**2/3**, respectively, correspond to the methyl migrations from the iron atom toward sulfur. The resulting $Fe(CH_3SH)^+$ complex is located at $E_{rel} = -1.05$ and -0.37 eV for ^{4}**3** and ^{6}**3**, respectively. The theoretical geometries of the CH_3SH moieties are very similar in both complexes (Chart 1); however, the Fe−S bond lengths differ in the two spin states, as expected for a change from a largely electrostatic interaction in the sextet state ($r_{FeS} = 2.45$ Å) to a dative bond in the quartet state ($r_{FeS} = 2.28$ Å). This is a consequence of the interaction between the S lone pair electrons and an occupied 4s orbital in $Fe^+(^6D)$ vs an empty 4s orbital for $Fe^+(^4F)$. The changes in the bonding situation can also explain the higher stability of ^{4}**3** over ^{6}**3**.

Reactions of the $HFeSCH_3^+$ Intermediate (Figure 3, Path ⓑ). This reaction proceeds from encounter complex **1** via TS**1/4** to the insertion intermediate **4**. To reach the TS, two types of motions have to occur: (i) methyl migration to the sulfur and (ii) hydrogen migration to iron. The sextet TS ($E_{rel} = 1.94$ eV) exhibits a structure where iron is almost inserted into a C−H bond of the methane molecule with calculated bond lengths $r_{FeC} = 2.03$ Å and $r_{FeH} = 1.60$ Å and a dihedral angle of $\theta_{HFeSC} = 76.3°$. The imaginary frequency of i212 cm^{-1} corresponds to the motion of the methyl group from iron to sulfur in conjunction with a methyl torsion. A comparable TS on the quartet surface could not be located despite an extensive search. Nevertheless, as a first approximation, a single-point calculation on the geometry of the sextet TS locates ^{4}TS**1/4** at $E_{rel} = 2.81$ eV. The frequency calculation, however, reveals two imaginary frequencies for this structure on the quartet PES (i559 and i153 cm^{-1}). The smaller corresponds to the motion and rotation of the methyl group in analogy to the sextet counterpart, while the larger corresponds to an increase of the HFeSC dihedral angle. Although the energy and structure of an optimized ^{4}TS**1/4** will most likely change somewhat, the TS seems to be located far above both the entrance channel and TS**1/2** of the pathway to generate the isomeric CH_3FeSH^+ insertion intermediate **2**. Therefore, the interconversion **1** → **4** is unlikely to play a role in the present experiments and is neglected in the overall interpretation of the data below.

The quartet and sextet states of the insertion intermediate **4**, $HFeSCH_3^+$, are located at $E_{rel} = 0.01$ and 0.09 eV, respectively. While ^{4}**4** is calculated to be nonplanar with a dihedral angle of $\theta_{HFeSC} = 75.2°$, the sextet structure ^{6}**4** shows a planar arrangement of this substructure, $\theta_{HFeSC} = 0.0°$. Given the similar energies of ^{6}**4** and ^{4}**4**, crossing between the sextet and quartet surfaces in this region of the PES is expected to be facile. From **4**, the reaction can continue via TS**3/4** toward the product complex **3**, described above. The sextet ^{6}TS**3/4** is located well above the entrance channel ($E_{rel} = 1.06$ eV) with an imaginary

mode of i1148 cm^{-1}, corresponding mainly to the hydrogen atom transfer from iron to sulfur. The situation is quite different in the quartet state. Despite numerous attempts to locate ^{4}TS**3**/**4** at the B3LYP/6-311+G* level of theory, no TS was found. The input structures collapsed during optimization to give ^{4}**3** or sometimes returned to ^{4}**4**, thus pointing to a very flat PES in this area. Vertical excitation from the ^{6}TS**3**/**4** geometry to the quartet surface yields a relative energy for the quartet TS of only −0.03 eV. Note that this value actually lies below the corresponding ^{4}**4** minimum. To obtain more information about the quartet region, the smaller 6-311G basis set was used in the calculations. At this level of theory, a stationary point ^{4}TS**3**/**4** is indeed found (see Chart 1). The frequency calculation for this geometry at the B3LYP/6-311G level of theory shows a single imaginary frequency of i393 cm^{-1}, corresponding to the migration of the iron-bound hydrogen atom to the sulfur. Using the B3LYP/6-311+G* approach, a single-point calculation reveals the TS to be located at $E_{rel} = 0.03$ eV, i.e., only about 0.02 eV above the minimum ^{4}**4**. Note, however, that a frequency calculation at this higher level of theory shows two imaginary frequencies (i557 and i139 cm^{-1}), where the larger corresponds to hydrogen migration from iron to sulfur and the smaller one represents a methyl torsion around the S−C axis. B3LYP/6-311+G* geometry optimizations starting at this point lead to a continuous decrease of both imaginary frequencies and convergence to the ^{4}**3** product complex. The close energies of ^{4}TS**3**/**4** and ^{4}**4** easily explain the difficulties encountered during localization of ^{4}TS**3**/**4**. We therefore deemed it unnecessary to further explore this part of the PES, as the barrier associated with ^{4}TS**3**/**4** seems to be small and similar to that found with the B3LYP/6-311G approach. Similar phenomena have also been observed in the theoretical investigations of the FeS^+/H_2 and ScS^+/H_2 systems,[13,36] in which the low-spin insertion intermediates do not represent true minima.

Products. Experimentally, Fe^+ and $FeSH^+$ are formed as major ionic products in the reaction of FeS^+ with CH_4, reactions 2 and 4. Minor ionic products, in their deuterated form, correspond to $FeCH_3^+$, $FeSCH_3^+$, and $FeSCH^+$, according to reactions 3, 5, and 6. Three processes by which the different products may be formed are considered: (i) dissociation of the insertion structure CH_3FeSH^+ into either $FeCH_3^+ + SH$ or $FeSH^+ + CH_3$, (ii) dissociation of $HFeSCH_3^+$ to yield $FeH^+ + CH_3S$ or $FeSCH_3^+ + H$, and (iii) dissociation of the product complex $Fe(CH_3SH)^+$ to form methanethiol and Fe^+, $FeSH^+ + CH_3$, or $FeSCH_3^+ + H$. Thus, our investigation includes the experimentally observed ionic products together with their neutral counterparts as well as formation of FeH^+ and CH_3S. Note, however, that loss of a methyl or hydrogen radical from **4**, $Fe(CH_3SH)^+$, is likely to be much less pronounced than elimination of the intact methanethiol molecule.[37,38] This is especially true because cleavage of the electrostatic bond between iron and methanethiol is expected to be more facile than cleaving the covalent S−C or S−H bonds.

In the following, the products are presented in the order of increasing molecular mass of the ionic species, starting with formation of $Fe^+(^6D)$ and methanethiol. The latter exhibits C_1 symmetry, and calculations give a carbon−sulfur bond length of 1.84 Å. The energy of the $^6Fe^+ + CH_3SH$ product channel is calculated as $E_{rel} = 0.98$ eV, and the corresponding quartet is corrected to the experimental state splitting 0.25 eV above this asymptote.

The second feasible product is $FeH^+ + CH_3S$ ($E_{rel} = 2.08$ eV), whose experimental counterpart FeD^+ was not observed. At the B3LYP/6-311+G* level of theory, the FeH^+ molecule has a quintet ground state ($^5\Delta$)[39] with a bond length of 1.58 Å; the lowest-lying triplet state ($^3\Pi$) is 1.39 eV higher in energy.[40] Another exit channel to be considered is $FeCH_3^+ + SH$ found at $E_{rel} = 1.61$ eV. In $FeCH_3^+$, the iron−carbon and carbon−hydrogen distances are computed as 1.91 and 1.10 Å, respectively. In the experiments, the deuterated analogue of this exit channel is observed as one of the minor channels. The complementary channel to form $FeSH^+ + CH_3$ is located at $E_{rel} = 1.06$ eV, i.e., only slightly higher than the lowest energy channel, $Fe^+(^6D)$ and CH_3SH. In addition to an $FeSH^+$ structure, the connectivity $SFeH^+$ is also conceivable and could result from breaking the carbon−sulfur bond in **4**, $HFeSCH_3^+$. Our calculations locate the ground state of the $SFeH^+$ isomer ($^3A'$) as 1.98 eV higher in energy than the $FeSH^+(^5A')$ ground state.[13]

The last exit channel accessible via a one-step reaction is formation of $FeSCH_3^+ + H$ ($E_{rel} = 1.56$ eV). For the $FeSCH_3^+$-(^{5}A) ground state, the calculations predict a bond dissociation energy of $D_0(Fe^+-SCH_3) = 3.03$ eV.[41] Other structural isomers for this species are also conceivable, for instance, with the connectivity $SFeCH_3^+$, $(CH_2S)FeH^+$, or $Fe(CH_2SH)^+$. The $SFeCH_3^+$ isomer could result from dissociation of intermediate **2**, CH_3FeSH^+, by breaking the hydrogen−sulfur bond. The $(CH_2S)FeH^+$ isomer could arise from loss of a hydrogen atom from the insertion intermediate **4**, $HFeSCH_3^+$. Further, an $Fe(CH_2SH)^+$ isomer can be accessed by H atom loss from the $Fe(CH_3SH)^+$ complex. All three isomers are somewhat unlikely to be formed as these pathways involve breaking strong covalent bonds (S−H[37] and C−H[42]) in the presence of bonds whose homolytic cleavage is less demanding energetically (Fe^+−C, Fe^+−H, and Fe^+−S). Our calculations confirm this intuitive assignment, showing that the lowest-lying electronic states of the $SFeCH_3^+$ and $(CH_2S)FeH^+$ structural isomers are located 0.42 and 1.01 eV above the ground-state $FeSCH_3^+$ isomer. Despite various attempts, no convergence was achieved for the putative $Fe(CH_2SH)^+$ isomer.

Experimentally, formation of the deuterated analogue of $FeSCH^+$ is observed as another product. According to the mechanistic scheme presented in Figure 3, we assume this product to be formed by loss of H_2 from $FeSCH_3^+$. To clarify the minimum structure of $FeSCH^+$, we briefly explored the $[Fe,C,S,H]^+$ surface using a lower level of theory, i.e., geometry optimizations using B3LYP with a very small 3-21G basis, and determination of relative energies by single-point calculations with B3LYP/6-311+G* (Table 3). (No frequency calculations were performed, such that relative energies for the $[Fe,C,S,H]^+$ species are not corrected for ZPVE.) At this level of theory, the most stable isomer is ^{3}**5**, in which iron, sulfur, and carbon

TABLE 3: Total Energies (E_{tot}) and Relative Energies (E_{rel}) of the $[Fe,C,S,H]^+$ Species[a]

species	spin state	E_{tot} (hartrees)	E_{rel} (eV)
5	3	1700.296 46	0.00
	5	1700.292 89	0.10
6	3	1700.256 49	1.09
	5	1700.245 86	1.38
7	3	1700.249 51	1.28
	5	1700.231 16	1.78
8	3	1700.210 64	2.33
	5	1700.199 11	2.65
9	3	1700.203 02	2.54
10	3	1700.264 77	0.86
	5	1700.281 99	0.39

[a] Values are calculated at the B3LYP/6-311+G*//B3LYP/3-21G level of theory. No frequency calculations were performed; hence, ZPVE corrections are not included.

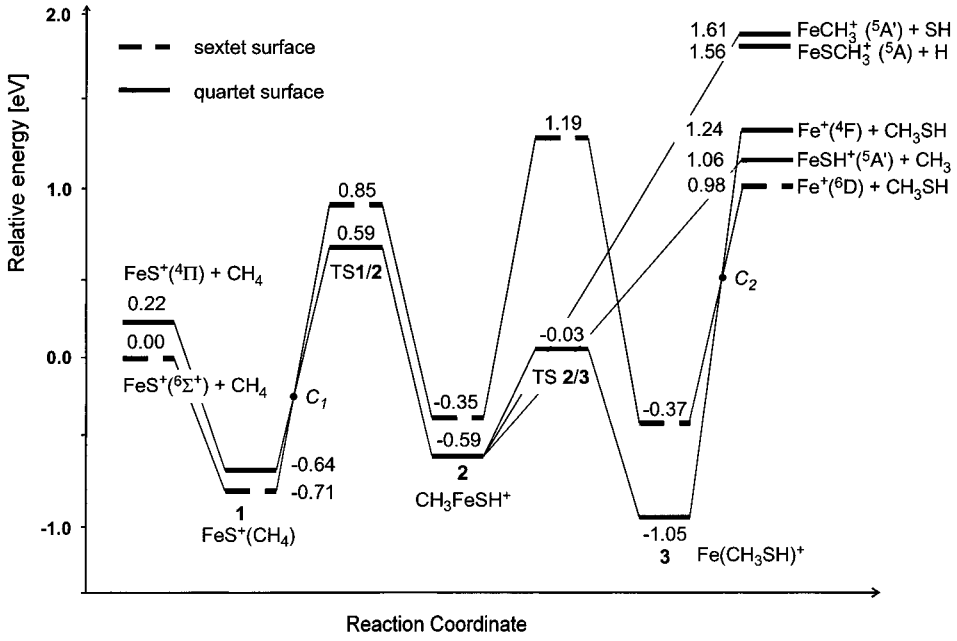

Figure 4. B3LYP/6-311+G* potential-energy surface for pathway ⓐ of the FeS^+/CH_4 system, involving intermediate formation of CH_3FeSH^+ (**2**). All energies are given in electronvolts relative to the entrance channel $FeS^+ + CH_4$ and include ZPVE contributions. The solid lines represent minima and transition structures along the quartet surface, while the dashed lines belong to the sextet surface. C_1 and C_2 denote the tentative crossing points between the sextet and the quartet surfaces; see the text.

CHART 2

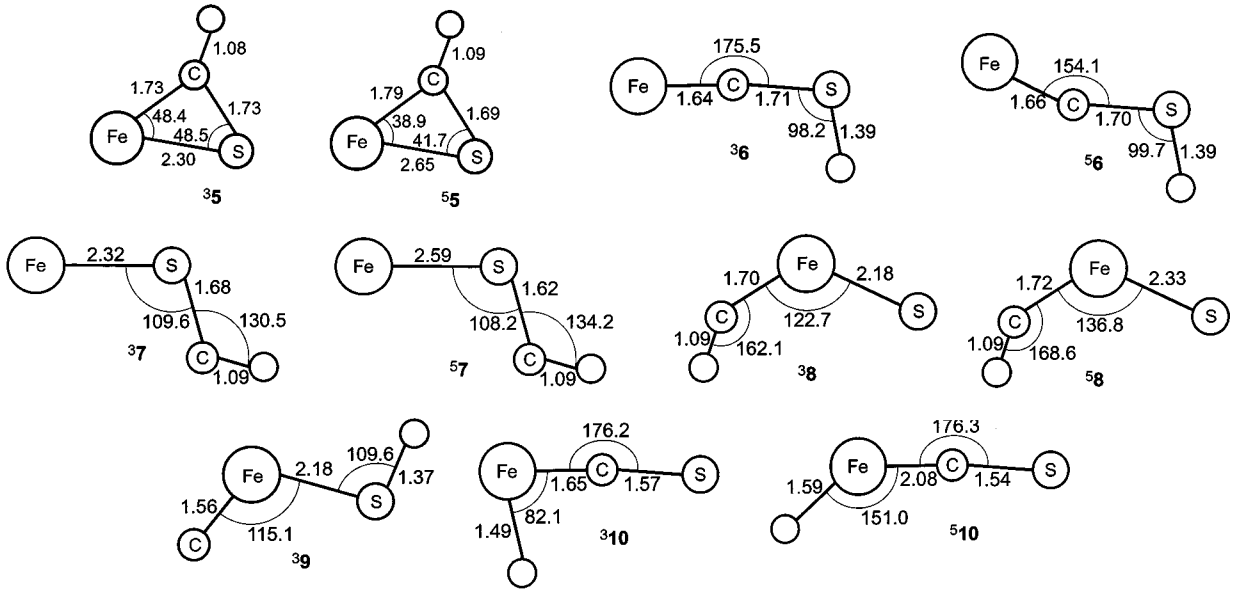

form a three-membered ring and the hydrogen atom is attached to the carbon atom in C_s symmetry (Chart 2). The corresponding quintet isomer ^{5}**5** is located only 0.10 eV above the triplet; thus, assignment of the ground state is ambiguous in this case. All other structural isomers are higher in energy compared to **5**. Complete geometry optimization of the ^{3}**5** and ^{5}**5** species at the B3LYP/6-311+G* level of theory results in only small changes in geometry and relative energies. For example, the difference between ^{3}**5** and ^{5}**5** amounts to 0.10 eV in the B3LYP/6-311+G*//B3LYP/3-21G approach compared to 0.09 eV at the B3LYP/6-311+G*//B3LYP/6-311+G* level of theory. Thus, the use of the small 3-21G basis appears reasonable for an exploration of the $[Fe,C,S,H]^+$ species. For the minimum energy structure, the calculations suggest a bond dissociation energy of $D_0(Fe^+-HCS) = 2.92$ eV. Regarding the ionization energies (IEs) of iron ($IE_{Fe} = 7.9$ eV) and the thioformyl radical HCS ($IE_{HCS} > 7.3$ eV),[43] it is not surprising that the positive charge is delocalized over the whole system as indicated by the Mulliken charge analysis, i.e., (Fe) +0.55, (C) +0.12, and (S) + 0.33, where the charge on the hydrogen atom is summed into that of carbon.

Discussion

Although the experiments are carried out using deuterated methane, only the PESs of the perprotio variants of the system are discussed (Figures 4 and 5), and relevant experimental values have been adjusted accordingly. In the construction of the PESs, only the most stable conformers are considered, because we assume the barriers for the interconversion of the electrostatically bound conformers to be much lower than the barriers associated with breaking and formation of covalent bonds. Also, the

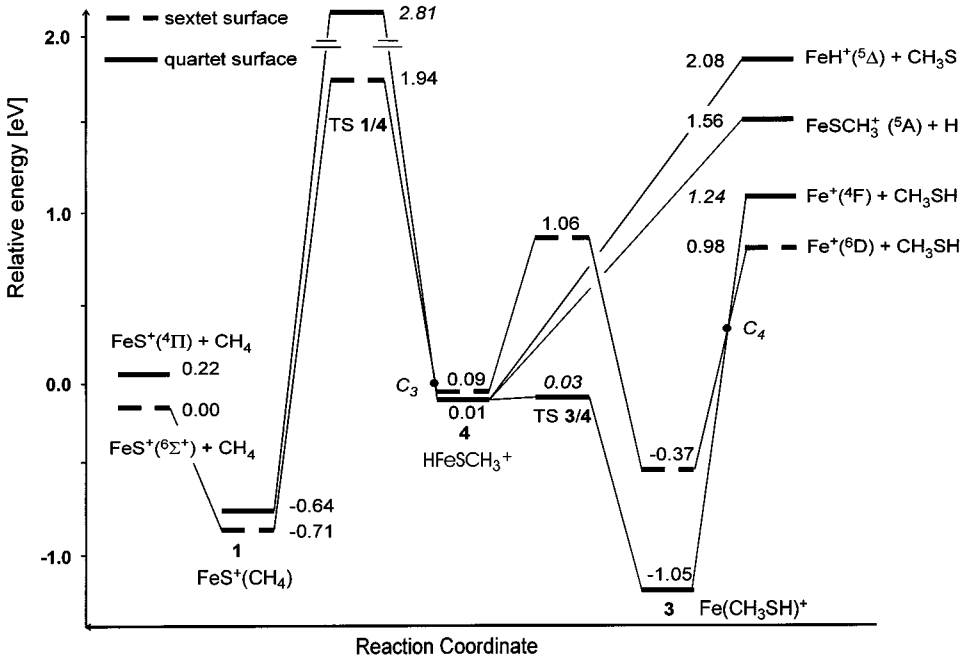

Figure 5. B3LYP/6-311+G* potential-energy surface for pathway ⓑ of the FeS^+/CH_4 system, involving intermediate formation of $HFeSCH_3^+$ (**4**). All energies are given in electronvolts relative to the entrance channel $FeS^+ + CH_4$ and include ZPVE contributions. The solid lines represent minima and transition structures along the quartet surface, while the dashed lines belong to the sextet surface. C_3 and C_4 denote the tentative crossing points between the sextet and the quartet surfaces. For further details on species such as ^{4}TS**1/4** and ^{4}TS**3/4**, see the text.

predicted barriers for the lowest-energy pathways are below the asymptotic energy of all products, such that theory predicts that the experimentally observed thresholds for all products will correspond to the thermochemical thresholds. Further, because B3LYP incorrectly predicts the state splitting of Fe^+ (see above), the experimental splitting is used in the construction of the PES.

Reaction via the CH_3FeSH^+ Intermediate (Figure 4). Within the ±0.3 eV error of the B3LYP approach, the calculated threshold of 0.98 eV for formation of Fe^+ agrees reasonably well with the threshold of 0.78 ± 0.12 eV obtained from literature thermochemistry (Table 1). The experimentally measured threshold of 1.11 ± 0.19 eV is somewhat larger than the thermodynamic threshold for formation of $Fe^+(^6D) + CH_3SH$, 0.78 ± 0.12 eV, but comparable to that for $Fe^+(^4F) + CD_3SD$, 1.03 ± 0.12 eV. This is consistent with the PES of Figure 4, which shows that formation of Fe^+ at low energies cannot occur by remaining on the sextet surface alone because ^{6}TS**2/3** is significantly above the exit channel. Instead, the reaction must cross to the quartet surface between the encounter complex **1** and the transition structure TS**1/2**;[44] for the sake of simplicity, we denote the multidimensional crossing seam by the point C_1 on this reaction coordinate diagram. The reaction then continues on the quartet surface from the low-lying ^{4}TS**1/2** (E_{rel} = 0.59 eV) to the insertion intermediate ^{4}**2**, CH_3FeSH^+. The latter may then rearrange to form the product complex ^{4}**3**, $Fe(CH_3SH)^+$, via ^{4}TS**2/3**. Formation of the ^{4}**3** product complex and further dissociation allow straightforward access to $Fe^+(^4F) + CH_3SH$ products. $Fe^+(^6D) + CH_3SH$ might also be formed, but this requires that the system recross to the sextet surface at the crossing seam denoted by point C_2 (Figure 4). Although this is possible, the energetic difference between ^{4}**3** and ^{6}**3** is much larger than between ^{4}**1** and ^{6}**1**. Thus, surface hopping in the exit channel is likely to be less efficient than in the entrance channel, because the larger state splitting would require formation of ^{4}**3** in higher vibrational levels, which are considered to have less favorable transition probabilities.[45]

The other major product at low energies can be formed in two ways. (i) The ^{4}**2** intermediate can dissociate into the $FeSH^+ + CH_3$ products, as well as $FeCH_3^+ + SH$. These channels are calculated to lie at E_{rel} = 1.06 and 1.61 eV, respectively, in good agreement with the experimental thermodynamic thresholds of 1.19 ± 0.17 and 1.68 ± 0.11 eV, respectively (Table 1). These simple bond fissions compete with the rearrangement to ^{4}**3**, and are kinetically favored. This partially explains why the cross section for $FeSD^+$ is larger than that of Fe^+ at the lowest energies (Figure 2). In addition, the relative magnitudes are most consistent with Fe^+ having a comparable onset to $FeSD^+$. This can again be rationalized by preferential formation of $Fe^+(^4F) + CH_3SH$ at 1.03 ± 0.12 eV relative to $FeSH^+ + CH_3$ at 1.19 ± 0.16 eV, but not by formation of $Fe^+(^6D) + CH_3SH$ at 0.78 ± 0.12 eV. The alternative dissociation pathway to form $FeCH_3^+ + SH$ requires higher energies, explaining the low intensity of the $FeCD_3^+$ product (Figure 1). (ii) Alternatively, the $Fe(CH_3SH)^+$ intermediate **3** can dissociate to form $FeSH^+ + CH_3$, by breaking the carbon−sulfur bond, and $FeSCH_3^+ + H$, by breaking the sulfur−hydrogen bond. Because the bond between Fe^+ and methanethiol is much weaker than the C−S or S−H bond, loss of CH_3SH is anticipated to be much more pronounced than loss of hydrogen or methyl radicals from the methanethiol unit. This certainly explains the low intensity of the $FeSCD_3^+$ cross section (Figure 1) and may suggest that (ii) is not the major pathway for formation of $FeSD^+$.

At higher energies, both the $FeSD^+$ and Fe^+ cross sections increase more rapidly. The rapid increase in Fe^+ starting near 3 eV is straightforwardly explained by reaction 2b. The explanation for the increase in $FeSD^+$, which has an approximate threshold between 2.5 and 3.1 eV (Figure 2), is not as obvious. One speculative explanation is that this is associated with a spin-allowed process occurring exclusively on the sextet surface (Figure 4), thereby explaining its larger magnitude. However, the apparent onset for this process is much higher than either calculated barrier on the sextet surface, TS**1/2** at E_{rel} = 0.85 eV or TS**2/3** at E_{rel} = 1.19 eV. Either the calculations significantly underestimate the barrier heights, the ability of the reaction system to surpass these barriers is not efficient until higher energies, or these higher energies are needed to efficiently

remain on the sextet surface at the C_1 crossing seam. An alternative explanation is to assign the increase in the $FeSD^+$ channel to several possible electronic or structural isomers. The calculations show, for instance, that besides the quintet ground state of $FeSH^+$, there exists a corresponding $FeSH^+$ triplet isomer, for which an energy splitting $^5FeSH^+/^3FeSH^+$ of 0.77 eV is obtained. Another structural isomer, $^5HFeS^+$, is also calculated 1.98 eV above $^5FeSH^+$. On the basis of these calculated values, these species could be formed starting at energies of 2.04 and 3.25 eV, respectively, in reasonable agreement with our observations.

In summarizing pathway ⓐ, we conclude that the reaction proceeding via intermediate **2**, CH_3FeSH^+, does explain formation of the experimentally observed products Fe^+, $FeSH^+$, $FeCH_3^+$, and $FeSCH_3^+$ easily. At threshold, preferential formation of excited-state $Fe^+(^4F)$ is indicated, and both the Fe^+ and $FeSH^+$ products have small magnitudes because the reactions are spin-forbidden; i.e., a curve-crossing at C_1 is needed. At higher energies, alternate and more efficient pathways become available for formation of Fe^+, the simple collision-induced dissociation process (2b), and of $FeSH^+$, possibly an excited state or isomer.

Reaction via the Intermediate $HFeSCH_3^+$ (Figure 5). In analogy to the predicted behavior for reaction of the FeS^+/CH_4 system along path ⓐ, the occurrence of path ⓑ involving intermediate **4**, $HFeSCH_3^+$, on the sextet surface is excluded from further consideration because of the substantially increased energy demands of both ^{6}TS**1/4** and ^{6}TS**3/4**. Moreover, reaction along the quartet surface is unlikely to occur because of the high-energy demand of ^{4}TS**1/4**. In good agreement with these calculations, formation of FeH^+, which is only conceivable via pathway ⓑ, is not observed at all in the experiments. Thus, the primary insertion reaction commences regioselectively by exclusive formation of intermediate **2**.

Finally, we briefly discuss the $[Fe,C,S,H]^+$ product channel. The energy behavior of the cross section for this reaction clearly shows that it is not a primary product, but rather stems from elimination of H_2 from the primary $FeSCH_3^+$ product. Whereas the $FeSCH_3^+$ channel rises somewhat earlier, it decreases dramatically as the $[Fe,C,S,H]^+$ product appears. At higher interaction energies (>7 eV) only formation of $[Fe,C,S,H]^+$ is observed, pointing to an increased reaction rate for the dehydrogenation and a corresponding decrease in lifetime of the $FeSCH_3^+$ product. It is also conceivable that $[Fe,C,S,H]^+$ is formed from primary loss of H_2, followed by loss of a H radical from the intermediate $FeSCH_2^+$. However, if the latter pathway were active, we would expect an $FeSCH_2^+$ product, which is not observed experimentally.

Conclusions

In the seemingly simple reaction of FeS^+ with CH_4, several ionic product species are observed experimentally. The experimental threshold for formation of Fe^+ at 1.11 ± 0.19 eV (after correction for ZPVE) agrees with the thermochemistry calculated from our B3LYP/6-311+G* approach as well as the literature thermochemistry for formation of $Fe^+(^4F) + CH_3SH$. For the $FeSH^+$ product, the data in the threshold region are noisy but consistent with appearance at the thermodynamic threshold. This agrees with literature thermochemistry and with B3LYP/6-311+G* calculations, which predict no barrier in excess of the endothermicity of this product channel. At higher energies, another process forming $FeSH^+$ more efficiently is observed, but has no easily assigned origin. Fe^+, formed by simple CID, dominates the reaction products at these elevated collision energies.

The results are in line with the occurrence of only one of the two theoretically investigated reaction mechanisms, i.e., pathway ⓐ via intermediate formation of CH_3FeSH^+ (**2**). The second pathway, which leads to the insertion isomer $HFeSCH_3^+$ (**4**) may be ruled out because of the high-energy demand associated with the C−H activation of methane via this route. In addition, along pathway ⓐ, participation of the sextet surface at low energies can be ruled out because of high barriers along this surface. Formation of Fe^+, accompanied by elimination of CH_3SH, is calculated to be the thermodynamically favored reaction, and accordingly, this product dominates in the experiments. $FeSH^+$ and $FeCH_3^+$ ions appear to be formed by direct dissociation of the CH_3FeSH^+ intermediate **2**, while formation of $FeSCH_3^+$ is best explained by breaking the sulfur−hydrogen bond in the product complex **3**, $Fe(CH_3SH)^+$.

Although the agreement between theory and experiment is quite good for most species, some shortcomings remain, e.g., the notoriously poor performance of the method in properly describing the sextet−quartet splitting between the ^{6}D and ^{4}F states of Fe^+. Despite these deficiencies, the present system constitutes yet another example where application of a reasonably economic level of theory provides valuable insight into the course of a reaction involving transition metals. This is especially significant because reactions involving open-shell transition-metal species still represent a considerable challenge to computational chemists and are difficult to treat with more sophisticated methods.[46]

Acknowledgment. This research was supported by the Deutsche Forschungsgemeinschaft, the Volkswagen-Stiftung, the Fonds der Chemischen Industrie, and the National Science Foundation. We thank Dr. Ilona Kretzschmar for helpful discussions and the Konrad-Zuse Zentrum Berlin for the generous allocation of computer time.

References and Notes

(1) Alpers, Ch. N., Blowes, D. W., Eds. *Environmental Geochemistry of Sulfide Oxidation*; ACS Symposium Series 550; American Chemical Society: Washington, DC, 1994.

(2) Stiefel, E. I., Matsumoto, K., Eds. *Transition-Metal Sulfur Chemistry*; ACS Symposium Series 653; American Chemical Society: Washington, DC, 1996.

(3) (a) Rodriguez, J. A.; Kuhn, M.; Hrbek, J. *Chem. Phys. Lett.* **1996**, *251*, 13. (b) Rodriguez, J. A.; Kuhn, M.; Hrbek, J. *J. Phys. Chem.* **1996**, *100*, 15494.

(4) Takakuwa, S. In *Organic Sulfur Chemistry, Biochemical Aspects*; Oae, S., Okyama, T., Eds.; CRC Press: Boca Raton, FL, 1992; p 1.

(5) (a) Kaim, W.; Schwederski, B. *Bioanorganische Chemie*; Teubner: Stuttgart, 1991. (b) Lippert, S. J.; Berg, J. M. *Principles of Bioinorganic Chemistry*; University Science Books: Mill Valley, CA, 1994. (c) Ogino, H.; Inomata, S.; Tobita, H. *Chem. Rev.* **1998**, *98*, 2093.

(6) (a) Harris, S. *Chem. Phys.* **1982**, *67*, 229. (b) Harris, S.; Chianelli, R. R. *Chem. Phys. Lett.* **1983**, *101*, 603. (c) Bauschlicher, C. W.; Maitre, P. *Theor. Chim. Acta* **1995**, *90*, 189.

(7) (a) Müller, A.; Diemann, E.; Jostes, R.; Bögge, H. *Angew. Chem.* **1981**, *93*, 957. (b) Carlin, T. J.; Wise, M. B.; Freiser, B. S. *Inorg. Chem.* **1981**, *20*, 2745. (c) Jackson, T. C.; Carlin, T. J.; Freiser, B. S. *Int. J. Mass Spectrom. Ion Processes* **1986**, *72*, 169. (d) McMahon, T. J.; Jackson, T. C.; Freiser, B. S. *J. Am. Chem. Soc.* **1989**, *111*, 421. (e) Dance, I. G.; Fisher, K. J.; Willett, G. D. *Angew. Chem., Int. Ed. Engl.* **1995**, *34*, 201. (f) Dance, I. G.; Fisher, K. J.; Willett, G. D. *Inorg. Chem.* **1996**, *35*, 4177. (g) Harvey, J. N.; Heinemann, C.; Fiedler, A.; Schröder, D.; Schwartz, H. *Chem. Eur. J.* **1996**, *2*, 1230. (h) Kretzschmar, I.; Fiedler, A.; Harvey, J. N.; Schröder, D.; Schwarz, H. *J. Phys. Chem. A* **1997**, *101*, 6252. (i) Kretzschmar, I.; Schröder, D.; Schwarz, H. *Int. J. Mass Spectrom. Ion Processes* **1997**, *167/168*, 103. (j) Fisher, K.; Dance, I.; Willett, G. *J. Chem. Soc., Dalton Trans.* **1998**, 975. (k) Kretzschmar, I.; Schröder, D.; Schwarz, H.; Rue, C.; Armentrout, P. B. *J. Phys. Chem. A* **1998**, *102*, 10060. (l) Kretzschmar, I. *Energetics and Reactivity of the Binary Transition-Metal Sulfides of the 2nd and 3rd Row*. Ph.D. Thesis, Technischen Universität Berlin, D83, Shaker-Verlag, Berlin, 1999. (m) Kretzschmar, I.; Schröder, D.; Schwarz, H.; Armentrout, P. B. In *Advances in Metal and Semiconductor Clusters*—

Metal-Ligand Bonding and Metal-Ion Solvation; Duncan, M. A., Ed.; JAI Press Inc.: Stanford, in press.

(8) For metal−sulfide clusters, see for example: (a) Ramli, E.; Rauchfuss, T. B.; Stern, C. L. *J. Am. Chem. Soc.* **1990**, *112*, 4043. (b) Nakat, J. H. E.; Dance, I. G.; Fisher, K. J.; Rice, D.; Willett, G. D. *J. Am. Chem. Soc.* **1991**, *113*, 5141. (c) Dehen, S.; Schäfer, A.; Ahlrichs, R.; Fenske, D. *Chem. Eur. J.* **1996**, *2*, 429. (d) Fisher, K.; Dance, I.; Willett, G.; Yi, M. *J. Chem. Soc., Dalton Trans.* **1996**, 709. (e) Nakajima, A.; Hayase, T.; Hayakawa, F.; Kaya, K. *Chem. Phys. Lett.* **1997**, *280*, 381. (f) Harvey, J. N.; Schröder, D.; Schwarz, H. *Inorg. Chim. Acta* **1998**, *273*, 111.

(9) (a) Eller, K.; Schwarz, H. *Chem. Rev.* **1991**, *91*, 1121. (b) Freiser, B. S. *J. Mass. Spectrom.* **1996**, *31*, 703. (c) Armentrout, P. B.; Kickel, B. L. In *Organometallic Ion Chemistry*; Freiser, B. S., Ed.; Kluwer: Dordrecht, The Netherlands, 1996.

(10) Schröder, D.; Schwarz, H. *Angew. Chem., Int. Ed. Engl.* **1995**, *34*, 1973 and references cited therein.

(11) (a) Shaik, S.; Danovich, D.; Fiedler, A.; Schröder, D.; Schwarz, H. *Helv. Chim. Acta* **1995**, *78*, 1393. (b) Harris, N.; Shaik, S.; Schröder, D.; Schwarz, H. *Helv. Chim. Acta* **1999**, *82*, 1784.

(12) Fisher, E. R.; Elkind, J. L.; Clemmer, D. E.; Georgiadis, R.; Loh, S. K.; Aristov, N.; Sunderlin, L. S.; Armentrout, P. B. *J. Chem. Phys.* **1990**, *93*, 2676.

(13) Bärsch, S.; Kretzschmar, I.; Schröder, D.; Schwarz, H.; Armentrout, P. B. *J. Phys. Chem. A* **1999**, *103*, 5925.

(14) (a) Ervin, K. M.; Armentrout, P. B. *J. Chem. Phys.* **1985**, *83*, 166. (b) Schultz, R. H.; Armentrout, P. B. *Int. J. Mass Spectrom. Ion Processes* **1991**, *107*, 29. (c) Schultz, R. H.; Crellin, K. C.; Armentrout, P. B. *J. Am. Chem. Soc.* **1991**, *113*, 8590. (d) Armentrout, P. B. In *Advances in Gas Phase Ion Chemistry*; Adams, N. G., Babcock, L. M., Eds.: JAI Press: Greenwich, CT, 1992; Vol. 1, p 83.

(15) Beyer, T.; Swinehart, D. F. *Comm. Assoc. Comput. Machines* **1973**, *16*, 379.

(16) Herzberg, G. *Molecular Spectra and Molecular Structure*, reprint edition; Krieger: Malabar, FL, 1989, Vol. I; 1991, Vol. III.

(17) Sunderlin, L. S.; Armentrout, P. B. *Int. J. Mass Spectrom. Ion Processes* **1989**, *94*, 149.

(18) (a) Dalleska, N. F.; Honma, K.; Armentrout, P. B. *J. Am. Chem. Soc.* **1993**, *115*, 12125. (b) Khan, F. A.; Clemmer, D. C.; Schultz, R. H.; Armentrout, P. B. *J. Phys. Chem.* **1993**, *97*, 7978. (c) Dalleska, N. F.; Honma, K.; Sunderlin, L. S.; Armentrout, P. B. *J. Am. Chem. Soc.* **1994**, *116*, 3519.

(19) Rodgers, M. T.; Armentrout, P. B. *J. Phys. Chem. A* **1997**, *101*, 2614.

(20) (a) Lee, C.; Yang, W.; Parr, R. G. *Phys. Rev. B* **1988**, *37*, 785. (b) Miehlich, B.; Savin, A.; Stoll, H.; Preuss, H. *Chem. Phys. Lett.* **1989**, *157*, 200. (c) Becke, A. D. *J. Chem. Phys.* **1993**, *98*, 5648.

(21) McLean, A. D.; Chandler, G. S. *J. Chem. Phys.* **1980**, *72*, 5639.

(22) (a) Wachters, A. J. H. *J. Chem. Phys.* **1972**, *52*, 1033. (b) Hay, P. J. *J. Chem. Phys.* **1977**, *66*, 4377.

(23) *Gaussian 94* (Revision A.1): Frisch, M. J.; Trucks, G. W.; Schlegel, H. B.; Gill, P. M. W.; Johnson, B. G.; Robb, M. A.; Cheeseman, J. R.; Keith, T. A.; Petersson, G. A.; Montgomery, J. A.; Raghavachari, K.; Al-Laham, M. A.; Zakrzewski, V. G.; Ortiz, J. V.; Foresman, J. B.; Cioslowski, J.; Stefanov, B. B.; Nanayakkara, A.; Challacombe, M.; Peng, C. Y.; Ayala, P. Y.; Chen, W.; Wong, M. W.; Andres, J. L.; Replogle, E. S.; Gomperts, R.; Martin, R. L.; Fox, D. J.; Binkley, J. S.; Defrees, D. J.; Baker, J.; Stewart, J. P.; Head-Gordon, M.; Gonzalez, C.; Pople, J. A., Gaussian Inc., Pittsburgh, 1995.

(24) (a) Gonzalez, C.; Schlegel, H. B. *J. Chem. Phys.* **1989**, *90*, 2154. (b) Gonzalez, C.; Schlegel, H. B. *J. Phys. Chem.* **1990**, *94*, 5523.

(25) Koch, W.; Holthausen, M. C. *A Chemist's Guide to Density Functional Theory*; Wiley-VCH: Weinheim, 2000.

(26) (a) Glukhovtsev, M. N.; Bach, R. D.; Nagel, C. J. *J. Phys. Chem. A* **1997**, *101*, 316. (b) Kellogg, C. B.; Irikura, K. K. *J. Phys. Chem. A* **1999**, *103*, 1150.

(27) (a) Gunnarson, O.; Jones, R. O. *Phys. Rev. B* **1985**, *31*, 7588. (b) Russo, T. V.; Martin, R. L.; Hay, P. J. *J. Chem. Phys.* **1994**, *101*, 7729. (c) Holthausen, M. C.; Heinemann, C.; Cornehl, H. H.; Koch, W.; Schwarz, H. *J. Chem. Phys.* **1995**, *102*, 4931. (d) Bauschlicher, C. W., Jr. *Chem. Phys.* **1996**, *211*, 163.

(28) Sugar, J.; Corliss, C. *J. Phys. Chem. Ref. Data* **1985**, *14* (Suppl. 2).

(29) Jackson, T. C.; Carlin, T. J.; Freiser, B. S. *Int. J. Mass Spectrom. Ion Processes* **1986**, *72*, 169.

(30) In ICR studies, we could reproduce this branching ratio quite well. Additionally, we observe formation of small amounts (<3%) of $FeCH_3^+$, $FeSH^+$, and $FeSCH_3^+$.

(31) (a) Kappes, M. M.; Staley, R. H. *J. Phys. Chem.* **1981**, *85*, 942. (b) Jackson, T. C.; Jacobson, D. B.; Freiser, B. S. *J. Am. Chem. Soc.* **1984**, *106*, 1252. (c) Schröder, D.; Schwarz, H. *Angew. Chem., Int. Ed. Engl.* **1990**, *29*, 1431. (d) Schröder, D.; Fiedler, A.; Hrusak, J.; Schwarz, H. *J. Am. Chem. Soc.* **1992**, *114*, 1215. (e) Baranov, V. I.; Javahery, G.; Hopkinson, A. C.; Böhme, D. K. *J. Am. Chem. Soc.* **1995**, *117*, 12801. (f) Schröder, D.; Schwarz, H.; Clemmer, D. E.; Chen, Y.; Armentrout, P. B.; Baranov, V. I.; Böhme, D. K. *Int. J. Mass Spectrom. Ion Processes* **1997**, *161*, 175.

(32) Note that the thresholds of CID processes depend on the collision gas. The most reliable thresholds are obtained with xenon as collision partner, while use of methane is known to give thresholds that are too high, thus agreeing nicely with the result for the second feature of the Fe^+ channel. For a discussion of several collision gases, see: (a) Aristov, N.; Armentrout, P. B. *J. Phys. Chem.* **1986**, *90*, 5135. (b) Hales, D. A.; Armentrout, P. B. *J. Cluster Sci.* **1990**, *1*, 127. (c) Reference 7k.

(33) (a) Yoshizawa, K.; Shiota, Y.; Yamabe, T. *Chem. Eur. J.* **1997**, *3*, 1160. (b) Yoshizawa, K.; Shiota, Y.; Yamabe, T. *J. Am. Chem. Soc.* **1998**, *120*, 564. (c) Yoshizawa, K.; Shiota, Y.; Yamabe, T. *Organometallics* **1998**, *17*, 2825. (d) Yoshizawa, K.; Shiota, Y.; Yamabe, T. *J. Chem. Phys.* **1999**, *111*, 538.

(34) Hübner, O.; Termath, V.; Berning, A.; Sauer, J. *Chem. Phys. Lett.* **1998**, *294*, 37.

(35) Bärsch, S.; Schröder, D.; Schwarz, H. *Helv. Chim. Acta* **2000**, *83*, 827.

(36) (a) Tilson, J. L.; Harrison, J. F. *J. Phys. Chem.* **1992**, *96*, 1667. (b) Tilson, J. L.; Harrison, J. F. *J. Phys. Chem.* **1991**, *95*, 5097.

(37) The bond strengths of the S−H and C−S bonds are estimated to be on the order of 3.7 and 3.0 eV, according to S−H and C−S bond strengths of comparable molecules, tabulated in ref 38. As references for the S−H bond strength, H−SH, H−SCH_3, and H−SC_6H_5 are used; for the C−S bond strength we refer to *t*-C_4H_9–SH, C_6H_5–SH, and CH_3–SC_6H_5.

(38) Weast, R. C., Ed. *CRC Handbook of Chemistry and Physics*; CRC Press Inc.: Boca Raton, FL, 1990.

(39) (a) Ohanessian, G.; Goddard, W. A., III. *Acc. Chem. Res.* **1990**, *23*, 386. (b) Petterson, L. G. M.; Bauschlicher, C. W.; Langhoff, S. R.; Partridge, H. *J. Chem. Phys.* **1987**, *87*, 481. (c) Carter, E. A.; Goddard, W. A., III. *J. Phys. Chem.* **1988**, *92*, 5679.

(40) McKee, M. L. *J. Am. Chem. Soc.* **1990**, *112*, 2601.

(41) The computational finding is supported by one of our FT-ICR experiments. Under thermal conditions ligand exchange was observed according to $FeCl^+ + CH_3SH \rightarrow FeSCH_3^+ + HCl$. The occurrence of this reaction leads to $D_0(Fe-SCH_3^+) \geq 2.86$ eV if the thermochemistry given in Table 1 is used.

(42) The C−H bond strength in a methyl group is given as 4.82 eV in ref 38.

(43) Ionization energies are taken from Lias, S. G.; Bartmess, J. E.; Liebman, J. F.; Holmes, J. L.; Levin, R. D.; Mallard, W. G. *Gas Phase* Ion and Neutral Thermochemistry. *J. Phys. Chem. Ref. Data* **1988**, *17* (Suppl. 1).

(44) The relevance of this type of crossing and the requirements for the violation of spin conservation have been discussed previously at great length; for details, see: (a) Elkind, J. L.; Armentrout, P. B. *J. Am. Chem. Soc.* **1986**, *108*, 2765. (b) Hanton, S. D.; Weisshaar, J. C. *J. Phys. Chem.* **1990**, *94*, 5655. (c) Armentrout, P. B. *Science* **1991**, *251*, 175. (c) Weisshaar, J. C. *Acc. Chem. Res.* **1993**, *26*, 213. (d) Filatov, M.; Shaik, S. *J. Phys. Chem. A* **1998**, *102*, 3538. (b) Reference 11. (c) Shaik, S.; Filatov, M.; Schröder, D.; Schwarz, H. *Chem. Eur. J.* **1998**, *4*, 193. (d) Plattner, D. A. *Angew. Chem., Int. Ed.* **1999**, *38*, 86. (e) Schröder, D.; Shaik, S.; Schwarz, H. *Acc. Chem. Res.* **2000**, *33*, 139.

(45) Rue, C.; Armentrout, P. B.; Kretzschmar, I.; Schröder, D.; Harvey, J. N.; Schwarz, H. *J. Chem. Phys.* **1999**, *110*, 7858.

(46) Brönstrup, M.; Schröder, D.; Kretzschmar, I.; Schwarz, H.; Harvey, J. N. *J. Am. Chem. Soc.*, in press.